

Supporting Information

Self-Sorting in the Formation of Metal–Organic Nanotubes: A Crucial Role of 2D Cooperative Interactions

Maiko Obana, Takahiro Fukino,* Takaaki Hikima, and Takuzo Aida*

*To whom correspondence should be addressed.

E-mail: fukino@macro.t.u-tokyo.ac.jp (T.F.); aida@macro.t.u-tokyo.ac.jp (T.A.)

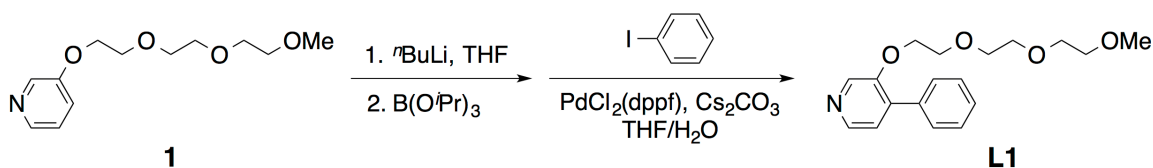
Table of Contents

1. General	S2
2. Synthesis	S3
3. NMR Spectroscopy	S4
4. Small Angle X-ray Scattering Analysis	S6
5. Transmission Electron Microscopy	S7
6. X-Ray Diffraction Analysis	S8
7. Evaluation of Formation Constants	S8
8. Statistical Prediction	S9
9. Supporting References	S10

1. General

All reagents were purchased from Kanto Chemical, Aldrich, Tokyo Chemical Industry (TCI), or Wako Pure Chemical Industries, and used as received without further purification unless otherwise noted. **FcL1**, **FcL2**, **L2**, and **1** were prepared according to reported procedures.^{S1} ¹H (500 MHz) and ¹³C NMR (126 MHz) spectra were recorded on a JEOL model JNM-ECA 500II spectrometer. Chemical shifts (δ) are reported in ppm relative to the internal standard tetramethylsilane ($\delta = 0.00$ ppm; ¹H NMR) or to the solvent signal of CDCl₃ ($\delta = 77.0$ ppm; ¹³C NMR). Matrix-assisted laser desorption/ionization time-of-flight mass (MALDI-TOF MS) spectrometry measurements were carried out on a Bruker Daltonics autoflexTM speed MALDI-TOF/TOF spectrometer using α -cyano-4-hydroxy cinnamic acid (CCA) as the matrix. Transmission electron micrographs (TEM) were recorded on a JEOL model JEM-1400 electron microscope operating at 120 kV. Samples were deposited on a Cu specimen grid, covered with thin polymer and carbon support films, manufactured by Okenshoji Co., Ltd. Small-angle X-ray scattering (SAXS) and 2D X-ray diffraction (2D XRD) experiments were carried out at the BL45XU beamline of SPring-8 (Hyogo, Japan)^{S2} using a Rigaku model R-Axis IV++ area detector. The scattering vector ($q = 4\pi\sin\theta/\lambda$) and the position of the incident X-ray beam on the detector were calibrated using several orders of layer reflections from silver behenate ($d = 58.380$ Å), where 2θ and λ denominate the scattering angle and the wavelength of the X-ray beam (1.0 Å), respectively. Sample-to-detector distances of 1.5 and 0.4 m were used for SAXS and 2D XRD measurements, respectively. Sample solutions for SAXS measurements were placed inside a metallic cell (thickness: 3 mm) with quartz windows. Recorded scattering/diffraction images were integrated along the Debye-Scherrer ring using the FIT2D software,^{S3} thus affording one-dimensional intensity data. Column chromatography on silica gel was performed on a Biotage Isolera Spektra equipped with a SNAP HP-Sil 10 g cartridge. Preparative HPLC was performed at room temperature using an ODS column (ϕ : 20 mm, length: 250 mm; Wakopak Wakosil-II 5C18 AR) on a Japan Analytical Industry model LC-9130 recycling preparative HPLC system.

2. Synthesis



Compound L1. To a THF solution (1.85 mL) of **1**^{S1} (400 mg, 1.66 mmol) was added a hexane solution (0.65 mL) of *n*BuLi (2.6 M, 1.66 mmol) under Ar at -78°C . The resulting mixture was stirred at -78°C for 10 min, then at 0°C for 10 min, and again cooled to -78°C . Subsequently, triisopropyl borate (457 mg, 2.43 mmol) was added, and then the reaction mixture was allowed to warm to 25°C , where it was stirred for 30 min. Then, water (0.15 mL) was added to the resulting suspension, and the mixture was stirred for 1 h at 25°C . To this reaction mixture were successively added iodobenzene (676 mg, 3.32 mmol) and Cs_2CO_3 (1.62 g, 4.97 mmol). After degassing via three freeze-pump-thaw cycles, $\text{PdCl}_2(\text{dppf})\cdot\text{CH}_2\text{Cl}_2$ (135 mg, 0.166 mmol) was added, and the resultant mixture was heated to reflux for 17 h. After cooling to 25°C , the reaction mixture was evaporated to dryness, and the resulting waxy residue was dissolved in CH_2Cl_2 and washed with water. The organic phase was separated, dried over anhydrous Na_2SO_4 , filtered, and evaporated to dryness. The obtained residue was subjected to column chromatography on silica gel ($\text{CH}_2\text{Cl}_2/\text{THF} = 92:8$ to $34:66$, v/v). The fraction containing the target compound was collected and evaporated to dryness. The residue was then subjected to recycling preparative HPLC on an ODS column with $\text{CH}_3\text{CN}/\text{MeOH}$ (10:1, v/v) as the eluent, which afforded **L1** as a colorless oil in 1.7% yield (9.0 mg, 0.031 mmol). ^1H NMR (500 MHz, CDCl_3): δ (ppm) 8.38 (br, 1H), 8.32 (br, 1H), 7.64–7.61 (m, 2H), 7.45–7.41 (m, 2H), 7.40–7.36 (m, 1H), 7.28 (br, 1H), 4.22 (t, $J = 5$ Hz, 2H), 3.80 (t, $J = 5$ Hz, 2H), 3.65–3.63 (m, 2H), 3.63–3.60 (m, 4H), 3.54–3.51 (m, 2H), 3.37 (s, 3H). ^{13}C NMR (126 MHz, CDCl_3): δ (ppm) 152.04, 143.27, 137.95, 136.16, 135.65, 129.27, 128.23, 128.18, 124.43, 71.89, 70.86, 70.65, 70.54, 69.55, 68.99, 59.02. HRMS (MALDI-TOF MS) m/z calcd. for $\text{C}_{18}\text{H}_{24}\text{NO}_4$ $[\text{M}+\text{H}]^+$: 318.1705; found: 318.1712.

3. NMR Spectroscopy

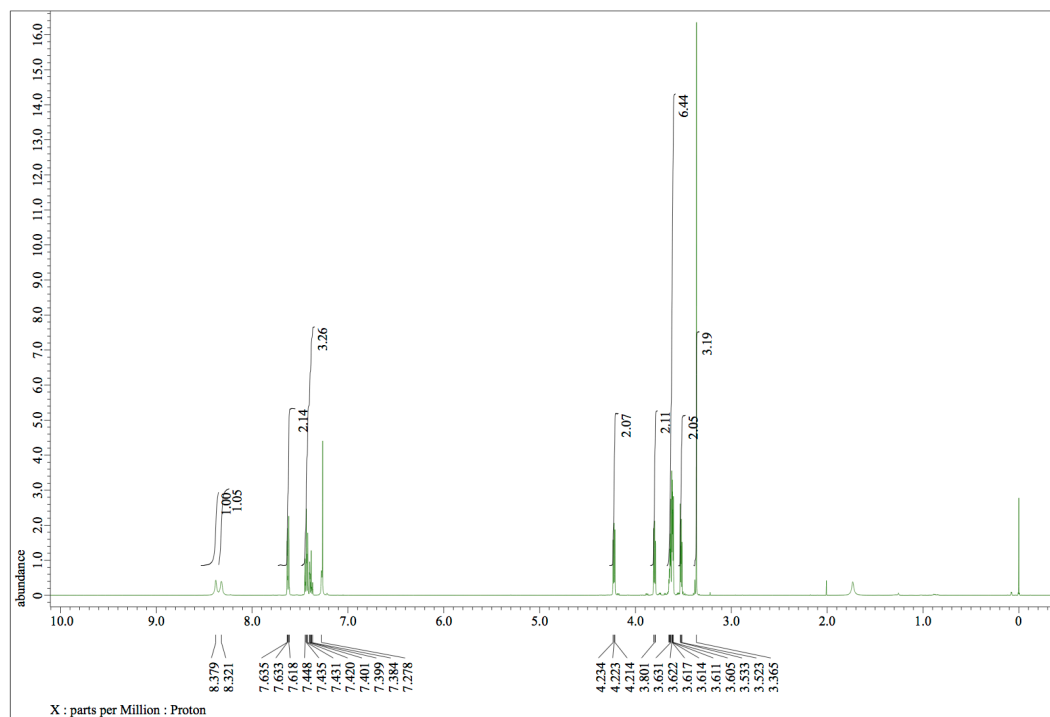


Figure S1. ^1H NMR (500 MHz) spectrum of L1 in CDCl_3 at 20°C .

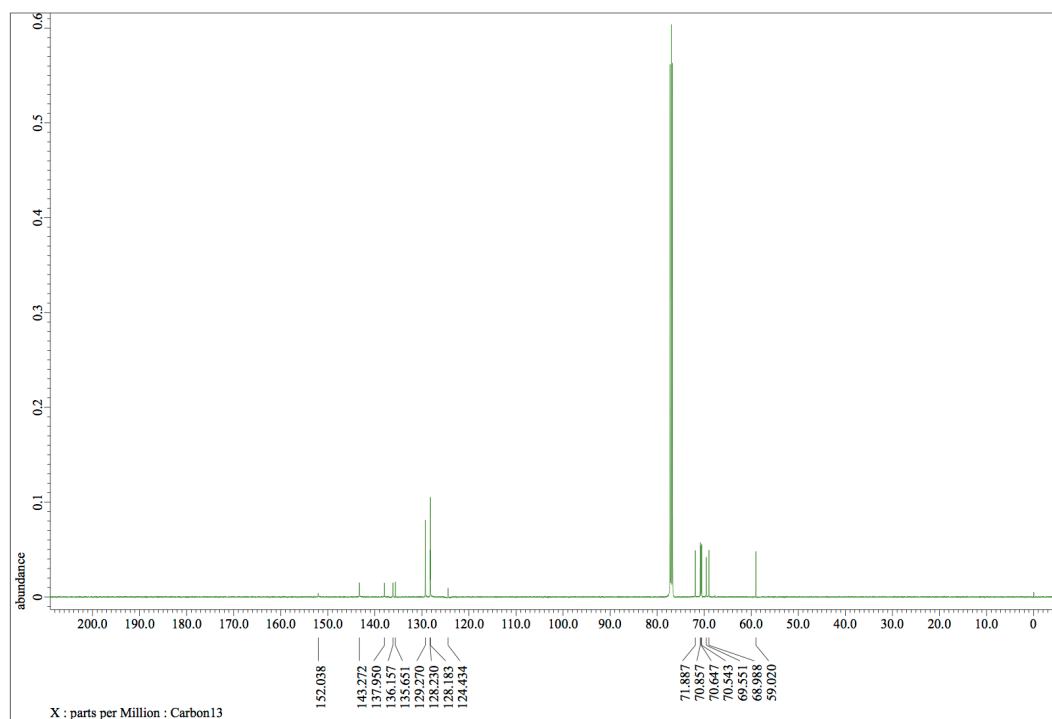


Figure S2. ¹³C NMR (126 MHz) spectrum of **L1** in CDCl₃ at 20 °C.

4. Small Angle X-ray Scattering Analysis

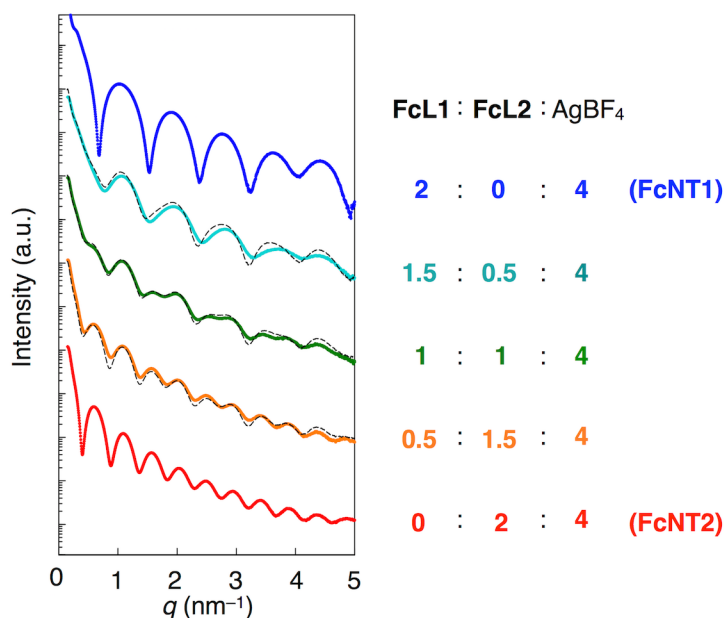


Figure S3. SAXS profiles of MeCN dispersions of **FcNT1** (blue) and **FcNT2** (red) as well as mixtures of **FcL1**, **FcL2**, and **AgBF₄** at molar ratios of 1.5:0.5:4 (cyan), 1:1:4 (green), and 0.5:1.5:4 (orange) (**[FcL1]** + **[FcL2]** = 10 mM, **[AgBF₄]** = 20 mM) at 20 °C. The broken curves superimposed on the cyan, green, and orange curves represent calculated profiles for mixtures of **FcNT1** (blue) and **FcNT2** (red) curves at ratios of 1.5:0.5, 1:1, and 0.5:1.5, respectively. For clarity, the scattering intensities at the molar ratios of 2:0:4 (blue), 1.5:0.5:4 (cyan), 0.5:1.5:4 (orange), and 0:2:4 (red) are offset by a factor of 10^4 , 10^2 , 10^{-2} , and 10^{-4} , respectively, and the broken curves superimposed on the cyan and orange curves are offset by the same factors as the corresponding intensities.

5. Transmission Electron Microscopy

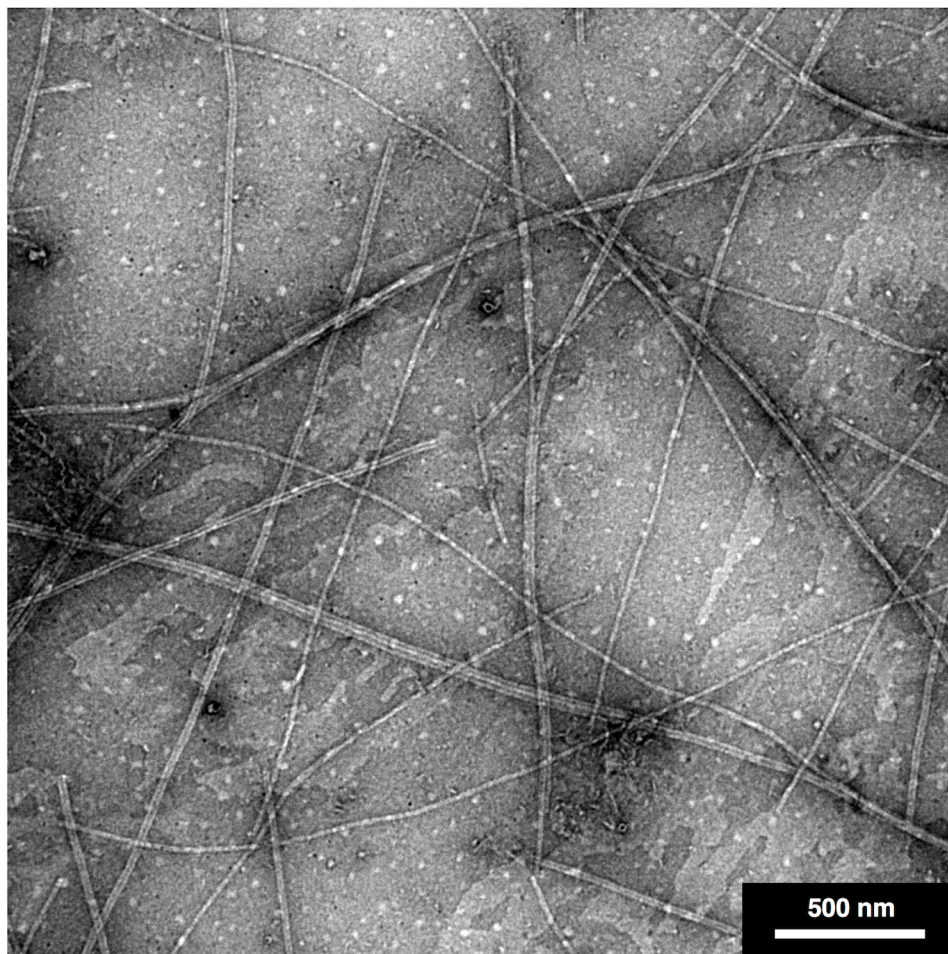


Figure S4. TEM image of an air-dried MeCN/EtOH/water dispersion of an assembled mixture of **FcL1**, **FcL2**, and AgBF_4 in MeCN ($[\text{FcL1}] = [\text{FcL2}] = 5.0 \text{ mM}$; $[\text{AgBF}_4] = 20 \text{ mM}$). The sample was negatively stained with uranyl acetate.

6. X-Ray Diffraction Analysis

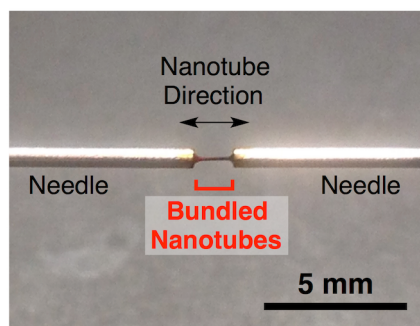


Figure S5. Photograph of the setup for air-dried sample preparation of unidirectionally orientated ferrocene-based metal–organic nanotubes for 2D XRD analysis (Figure 4).

Table S1. Parameters of simplified atomistic models used for simulation of 2D XRD patterns in the HELIX program^{S4} (Figure 4).

Corresponding Nanotube	Geometry	Radial Position (nm)	Axial Separation (nm)	Rotation Angle (degree)
FcNT1	Helix	3.7	0.70	4
FcNT1	Non-Helix	3.7	0.70	0
FcNT2	Helix	6.7	0.68	4
FcNT2	Non-Helix	6.7	0.68	0

7. Evaluation of Association Constants

Association constants for $[\text{Ag}(\text{L})]^+$ and $[\text{Ag}(\text{L})_2]^+$ ($\text{L} = \text{L1}$ and L2) were obtained from applying a nonlinear curve-fitting method using the WinEQNMR2 program^{S5} to chemical shift changes of the signals associated with the pyridyl α -protons of L upon titration of L with AgBF_4 in CD_3CN (Figure 4). As $\text{Ag}(\text{I})$ ions and pyridine derivatives form 1:2 complexes in CH_3CN ,^{S6} a 1:2 complexation model was employed for the analysis.

8. Statistical Prediction

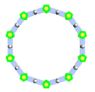

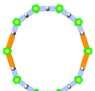
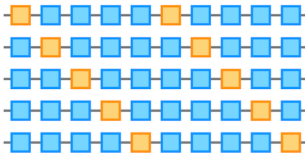
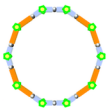
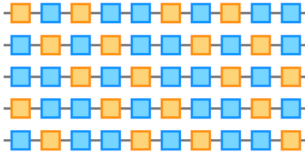
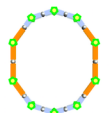
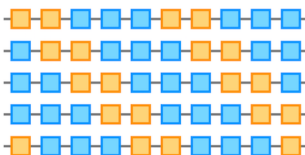
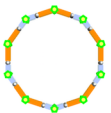

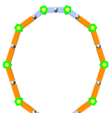
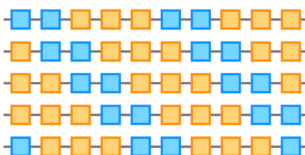
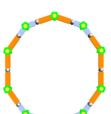
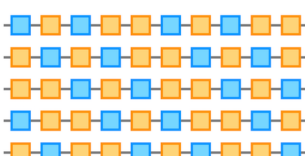
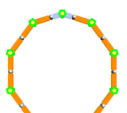
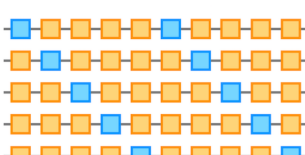
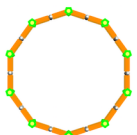

FcL1:FcL2 Ratio	Symmetry	Possible Cross-sectional Model	Possible Sequence	Probability of Occurrence
10:0	C_{10}		<div>1 2 3 4 5 6 7 8 9 10</div> 	$\frac{1}{1024}$
8:2	C_2			$\frac{5}{1024}$
6:4	C_2			$\frac{5}{1024}$
6:4	C_2			$\frac{5}{1024}$
5:5	C_5			$\frac{2}{1024}$
4:6	C_2			$\frac{5}{1024}$
4:6	C_2			$\frac{5}{1024}$
2:8	C_2			$\frac{5}{1024}$
0:10	C_{10}			$\frac{1}{1024}$

Figure S6. Statistical probabilities of decagonal cross sections of possible nanotubes.

9. Supporting References

- (S1) Fukino, T.; Joo, H.; Hisada, Y.; Obana, M.; Yamagishi, H.; Hikima, T.; Takata, M.; Fujita, N.; Aida, T. *Science* **2014**, *344*, 499.
- (S2) Fujisawa, T.; Inoue, K.; Oka, T.; Iwamoto, H.; Uruga, T.; Kumasaka, T.; Inoko, Y.; Yagi, N.; Yamamoto, M.; Ueki, T. *J. Appl. Crystallogr.* **2000**, *33*, 797.
- (S3) <http://www.esrf.eu/computing/scientific/FIT2D/>
- (S4) Knupp, C.; Squire, J. M. *J. Appl. Crystallogr.* **2004**, *37*, 832.
- (S5) Hynes, M. J. *J. Chem. Soc., Dalton Trans.* **1993**, 311.
- (S6) (a) Di Bernardo, P.; Melchior, A.; Portanova, R.; Tolazzi, M.; Zanonato, P. L. *Coord. Chem. Rev.* **2008**, *252*, 1270. (b) Ignaczak, M.; Grzejdziak, A. *Monatsh. Chem.* **1984**, *115*, 943.